NANO LETTERS

2006
Vol. 6, No. 10
2313−2317

Strain-Induced Self Organization of Metal–Insulator Domains in Single-Crystalline VO_2 Nanobeams

Junqiao Wu,[†,‡] Qian Gu,[†,‡] Beth S. Guiton,[‡] Nathalie P. de Leon,[‡] Lian Ouyang,[‡] and Hongkun Park*[,‡,§]

Department of Chemistry and Chemical Biology and Department of Physics, Harvard University, 12 Oxford Street, Cambridge, Massachusetts 02138

Received August 5, 2006; Revised Manuscript Received September 14, 2006

ABSTRACT

We investigated the effect of substrate-induced strain on the metal–insulator transition (MIT) in single-crystalline VO_2 nanobeams. A simple nanobeam–substrate adhesion leads to uniaxial strain along the nanobeam length because of the nanobeam's unique morphology. The strain changes the relative stability of the metal (M) and insulator (I) phases and leads to spontaneous formation of periodic, alternating M–I domain patterns during the MIT. The spatial periodicity of the M–I domains can be modified by changing the nanobeam thickness and the Young's modulus of the substrate.

Many unique properties of transition metal oxides, including ferroelectricity,[1,2] colossal magnetoresistivity,[3−5] and high-T_C superconductivity,[6] originate from the interplay between structural phase transitions and nanoscale electronic and magnetic ordering. Lattice strain, which affects the relative stability of competing structural phases, thus has a profound influence on the electrical, optical, and magnetic properties of these oxides.[1−6] Coherent strain generated from epitaxial growth can result in spontaneous formation of domain patterns in single crystals and thin films[2,7−14] and can also be used to change the thermodynamic stability of distinct functional phases in ferroelectric[1] and superconducting[6] thin films.

Bulk vanadium dioxide (VO_2) undergoes a Mott metal−insulator transition (MIT) at $T_{C,bulk} \approx 68$ °C[15−17] and has been suggested as a candidate for realizing Mott field-effect transistors[18,19] and thermochromic devices.[20,21] The MIT in VO_2 is accompanied by a structural phase transition from a low-temperature (semiconducting or insulating) monoclinic lattice to a high-temperature (metallic) tetragonal lattice.[15,16] The relationship between this structural phase transition and the Mott MIT has been the subject of many experimental[19,22,23] and theoretical investigations.[15−17]

Here we report an experimental study on the effect of substrate-induced strain on the Mott MIT[15−17] in single-crystalline VO_2 nanobeams. Combined electrical, optical, and scanned probe investigations reveal that a simple adhesive interaction between the nanobeam and the substrate leads to a coherent uniaxial strain on the nanobeam. The resulting strain causes spontaneous formation of alternating nanoscale metal (M)−insulator (I) domains along the nanobeam length and thus produces nanoscale M−I heterostructures within a compositionally homogeneous material.[24] The present study demonstrates that VO_2 nanobeams behave as a one-dimensional system for M/I domain organization and that the spatial periodicity of M/I domains can be modified by changing the thickness of the nanobeam and the elasticity of the substrate. As such, it suggests a new strategy for strain engineering without the need for epitaxial growth.

Single-crystalline VO_2 nanobeams were prepared using a variant of the vapor transport method reported previously (see the Supporting Information).[25] Typical thicknesses of these nanobeams ranged from 30 to 500 nm, and their lengths reached more than 50 μm. Figure 1a shows a transmission electron microscopy image of a representative VO_2 nanobeam. Electron (Figure 1a, lower inset) and X-ray diffraction studies show that the single-crystalline VO_2 nanobeams possess a monoclinic structure at room temperature. The nanobeam morphology with a rectangular cross section arises from the preferential growth of VO_2 along the monoclinic [100] direction, with crystallographically equivalent $(01\bar{1})$ and (011) facets forming the sidewalls.[25]

The Mott MIT in the VO_2 nanobeams was studied by incorporating individual nanobeams into a four-probe geometry using electron-beam lithography and measuring their electrical characteristics as a function of temperature, T (see

* To whom correspondence should be addressed. E-mail: Hongkun_Park@harvard.edu.
† These authors contributed equally to this work.
‡ Department of Chemistry and Chemical Biology.
§ Department of Physics.

10.1021/nl061831r CCC: $33.50
Published on Web 09/26/2006

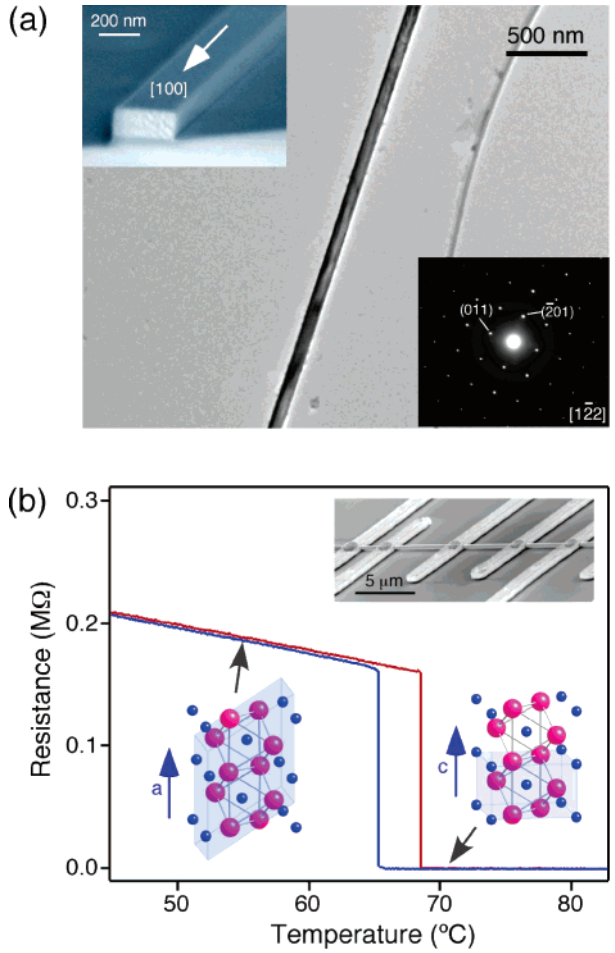

Figure 1. (a) Transmission electron microscopy (TEM) image of a representative VO_2 nanobeam. Upper inset, cross-sectional scanning electron microscopy (SEM) image of a VO_2 nanobeam as grown on a SiO_2 surface. Lower inset, selected area electron diffraction (SAED) pattern indexed for monoclinic VO_2 along the [1$\bar{2}$2] zone axis. The SAED pattern remains unchanged as the electron beam spot moves along the nanobeam, indicating that the whole nanobeam is a single crystal. (b) Resistance of a suspended VO_2 nanobeam measured in a four-probe geometry as a function of temperature. Red and blue curves are taken during heating and cooling, respectively. Upper inset, SEM image of the device with a VO_2 nanobeam suspended by ~200 nm from the SiO_2 surface. Schematic cartoons indicate the crystal structures of the low-temperature, monoclinic (left), and high-temperature, tetragonal (right) phases. Blue indicates V atoms, and magenta indicates O atoms. The unit cell is shaded in each case.

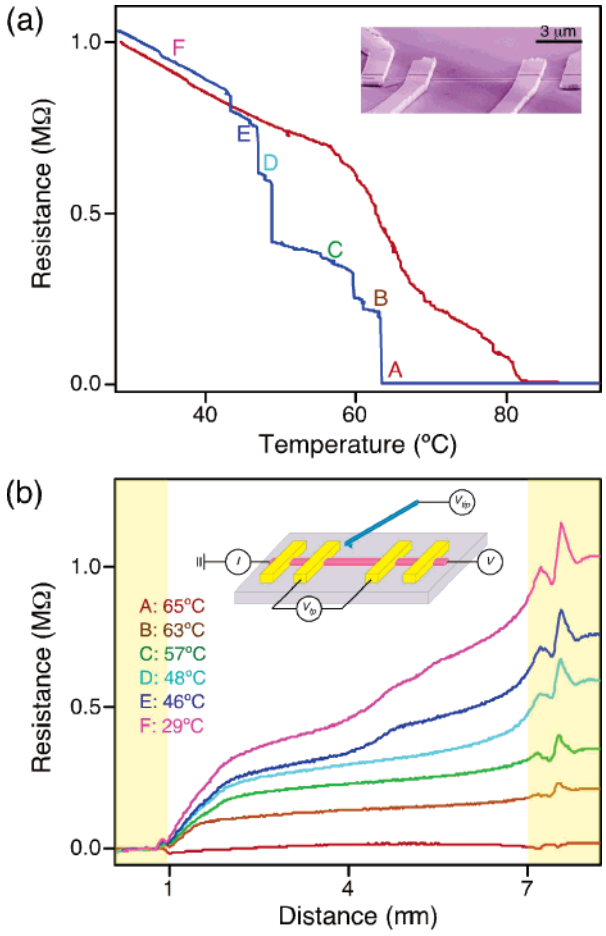

Figure 2. (a) Resistance of an on-substrate VO_2 nanobeam measured in a four-probe geometry as a function of temperature. Red and blue curves are taken during heating and cooling, respectively. Inset, SEM image of the on-substrate VO_2 nanobeam device. The height and width of this nanobeam are 100 and 210 nm, respectively. (b) Resistance profile along the nanobeam length obtained from the same device as in Figure 2a using Kelvin probe microscopy (KPM) at selected temperatures indicated in Figure 2a. The shaded areas on the sides indicate the electrode. On the curves in b, regions with steeper gradient are insulating (I) domains. In curve C, a new I domain appeared at the distance of ~1.7 μm, next to but separated from the existing I domain. Inset, a schematic of KPM applied to a four-probe device. V is the DC bias applied to the nanobeam, I is the current, V_{fp} is the measured four-probe voltage drop between the inner electrodes, and V_{tip} is the voltage applied to the cantilever (the sum of an AC signal at the cantilever resonance frequency and a DC voltage applied by the feedback loop).

the Supporting Information). Two distinct types of devices have been fabricated: in the first type, "suspended devices" (inset of Figure 1b), an individual VO_2 nanobeam is suspended from the substrate by metal electrodes,[26] whereas in the second type, "on-substrate devices" (inset of Figure 2a), a nanobeam is in contact with the SiO_2 substrate throughout its length.

Figure 1b shows a plot of the four-probe resistance versus T obtained from a suspended nanobeam device. The resistance of the device changed by a factor of $>10^4$ at $T_{C,bulk} \approx 68$ °C and exhibited a clear hysteresis during the temperature cycle. These characteristics are prototypical signatures of a first-order MIT[15] and were observed in more than 30 suspended nanobeam devices studied to date. Notably, the resistance changes signifying the MIT in these devices occurred within a temperature range <0.1 °C in both the heating and cooling half cycles, much sharper than the >1°C range observed in VO_2 thin films.[19,27,28]

Devices fabricated with VO_2 nanobeams lying on SiO_2 substrates exhibited markedly different resistance behavior upon temperature cycling, as illustrated in Figure 2a. The four-probe resistance of such an on-substrate device changed in many discrete steps over a much wider temperature range during heating and/or cooling half cycles. Essentially all (>100) on-substrate devices exhibited similar resistance jumps with various sizes and temperature positions. For a given device, the sizes and positions of the resistance jumps

were reproducible in subsequent thermal cycles and were independent of the T ramping rate (2 °C/min to 60 °C/min).

Figure 2b shows the temperature dependence of the resistance profile along the nanobeam length measured from the same device as in Figure 2a by Kelvin probe microscopy (KPM: see the Supporting Information).[29] Because of the capacitive coupling between the scanning tip and the nanobeam/electrode system, the effective potential (and hence the resistance profile) recorded by KPM is a weighted average of the surface potential from regions directly below the tip and those farther away.[30,31] Because of this lateral averaging effect, Figure 2b can only be used to distinguish domains with distinct resistivities relative to each other, and the absolute values of the slopes are not an accurate representation of the domain resistivity. At high temperatures (T > 65 °C), the resistance profile across the device was flat, indicating that the whole nanobeam was metallic. Whenever the four-probe resistance increased by a step in Figure 2a, a new, highly resistive region appeared along the nanobeam length, signifying the formation of a new insulating (I) domain. Figure 2b also shows that metallic (M) domains persist at temperatures well below $T_{C,bulk}$ (even down to room temperature), indicating the variation of phase transition temperatures (T_C) along the nanobeam length. Again, the positions of the M and I domains remained the same upon repeated temperature sweeps in a given device.

The MIT in VO_2 nanobeams can also be investigated without metal contacts by optical microscopy, exploiting the distinct light scattering properties of M and I phases.[11,20,21,23] Optical imaging of suspended nanobeam devices exhibited an immediate color change from bright (dark) to dark (bright) upon the abrupt resistance decrease (increase) at the MIT, allowing the identification that the bright (dark) color corresponds to the I (M) phase (see the Supporting Information). The suspended nanobeams did not show any domain structure. Figure 3a shows an optical micrograph of as-grown VO_2 nanobeams on a SiO_2 surface recorded at T = 100 °C. Each nanobeam exhibited a striking periodic bright−dark pattern that persists between ~70 °C and ~150 °C. As the temperature was raised (lowered), the dark (bright) domains grew in size along the nanobeam length. At T < 70 °C the nanobeams were all bright, whereas at T > 150 °C they were all dark. The positions of these domains remained highly reproducible upon repeated thermal cycling.

Comparison of Figure 1 with Figures 2 and 3 clearly shows that the nanobeam−substrate interactions affect the MIT in VO_2 nanobeams profoundly, causing the modification of their thermodynamic stability as well as spontaneous M−I domain formation. These observations can be understood by considering the structural change accompanying the MIT: as VO_2 changes from a tetragonal M to a monoclinic I phase, the lattice constant along the tetragonal c axis (or equivalently the monoclinic a axis) expands by ~1%.[20] Consequently, a tensile (compressive) stress along the tetragonal c direction stabilizes the I (M) phase, leading to the upward (downward) shift of the phase transition temperature, T_C.[27,28]

The observation of the I phase well above $T_{C,bulk}$ in Figure 3a is thus consistent with the tensile stress on as-grown VO_2 nanobeams arising from the mismatch of thermal expansion between VO_2 and SiO_2[32] at the growth temperature of 1100 °C (see the Supporting Information). Moreover, the periodic domain pattern in Figure 3a indicates that the adhesion between the as-grown nanobeams and the substrate is homogeneous along the nanobeam. By contrast, in on-substrate devices the temperature range in which the domain patterns appeared varied from device to device, and the domain patterns were irregular: these variations are most likely due to the fact that the nanobeams were mechanically transferred to the substrate during the device fabrication process and thus the stress distribution felt by the nanobeam was not uniform. In both cases, the locations of M−I domains are most likely determined by the specifics of the nanobeam−substrate interactions.

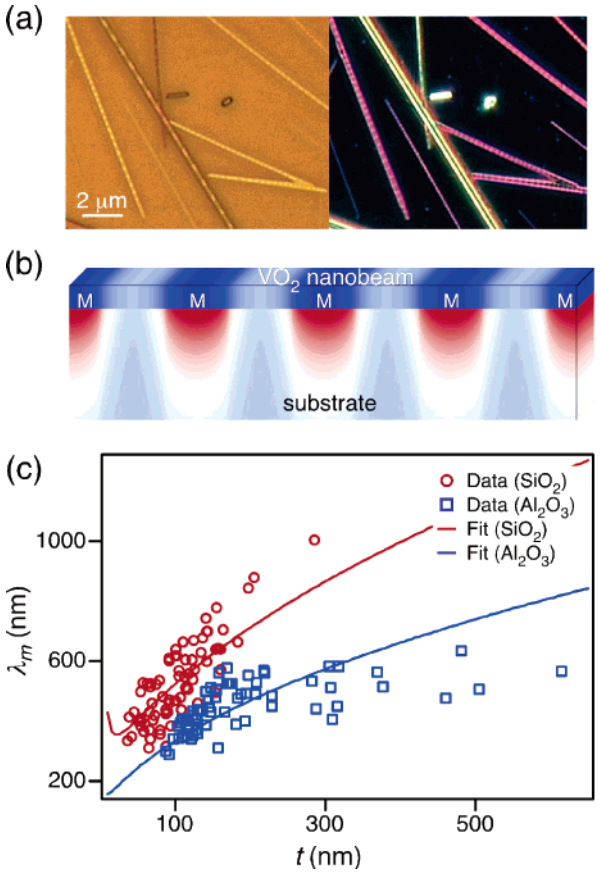

Figure 3. (a) Bright (left) and dark (right) field optical images of VO_2 nanobeams grown on a SiO_2 surface recorded at T = 100 °C during cooling in air. (b) Schematic diagram showing the periodic domain pattern of a VO_2 nanobeam strained on a SiO_2 substrate. Blue and red correspond to tensile and compressive strain, respectively. "M" denotes metallic phase, and the unlabeled intervening regions are I phase. (c) Spatial periods (λ_m) of the domain patterns as a function of the nanobeam thickness (t) for VO_2 nanobeams embedded in SiO_2 and Al_2O_3. Solid lines present the result of the theoretical fit described in the main text. The embedded nanobeam samples were prepared by first growing VO_2 nanobeams on SiO_2 and Al_2O_3 substrates and then covering them with ~100 nm SiO_2 and Al_2O_3, respectively. The nanobeam thicknesses were determined by atomic force microscopy before the SiO_2 and Al_2O_3 coating, and λ_m was determined by optical imaging. All experimental data were taken at T = 100 °C during the cooling half cycle. At this temperature, the M and I phases coexisted in equal fraction.

The periodic domain pattern seen in Figure 3a is reminiscent of, but much more regular than, those observed in elastic-misfit heterostructures, such as strained ferroelectrics,[2,7−9] epitaxial semiconductor films,[33] bulk VO_2 single crystals,[10−13] and magnetoresistive complex oxides.[14] The observed domain pattern can be explained by the competition between the domain-wall energy and the elastic energy of the nanobeam−substrate system. In these systems, a periodic domain pattern forms spontaneously during the structural phase transition because it represents the lowest-energy compromise between the elastic energy that favors domain formation and the domain wall energy that opposes it.

The spatial periodicity of the M−I domain patterns in Figure 3a can be described quantitatively using a model originally developed for the strained ferroelectric system.[9] Because the nanobeam length direction coincides with the tetragonal *c* axis, the nanobeam−substrate interaction naturally leads to a significant strain accumulation only along the tetragonal *c* direction. Moreover, in the temperature range between 90 and 110 °C in which the data in Figure 3 were obtained, the spatial period, λ, of the M−I domain pattern was not sensitively dependent upon temperature, and the ratio of the M and I domain lengths was very close to 1. The situation can therefore be approximated as a VO_2 nanobeam embedded in an elastic matrix with M and I phases coexisting in equal fraction, and the total energy, *E*, in unit nanobeam−substrate interface area is given by[9]

$$E(\lambda) = \frac{\lambda\epsilon}{\pi^3}\sum_{j=0}^{\infty}\frac{1-e^{-2(2j+1)\pi t/\lambda}}{(2j+1)^3} + \frac{\gamma t}{\lambda} + \frac{(f_M + f_I)t}{2} \qquad (1)$$

Here λ is the spatial period of the domain pattern, $\epsilon \approx Y(\Delta c/c)^2/2(1-\nu^2)$ is the volume density of the elastic misfit energy, *Y* is the effective Young's modulus of the system, $\Delta c/c \approx 0.011$ is the elongation percentage along the tetragonal *c* axis of VO_2 during the MIT, ν is the Poisson's ratio, γ is the domain-wall energy per unit domain-wall area, *t* is the nanobeam thickness, and f_M and f_I are the free energy densities of the M and I phases, respectively. The first term in eq 1 represents the elastic energy of a combined VO_2−substrate system, and the second term accounts for the domain wall energy. Given the energy expression in eq 1, the equilibrium domain period (λ_m) at each *t* can be determined by numerical minimization of $E(\lambda)$. Equation 1 also indicates that λ_m can be controlled by varying *Y* of the substrate.

Figure 3c shows the experimentally determined λ_m as a function of *t* for VO_2 nanobeams embedded in SiO_2 and Al_2O_3, and demonstrates that λ_m is indeed dependent on *t* and the matrix surrounding the nanobeams. The solid lines in Figure 3c are the results of a simultaneous fit to eq 1 of both data sets with γ as the only adjustable parameter and demonstrate that eq 1 provides a good description of experimental data. In this fit, *Y* for the VO_2−substrate system was approximated by taking the numerical average for those of VO_2 ($Y \approx 140$ GPa)[34] and the substrate ($Y(SiO_2) \approx 70$ GPa [34] $Y(Al_2O_3) \approx 306$ GPa [35]) because eq 1 assumes the same *Y* for the nanobeam and the surrounding medium. The effect of the *Y* anisotropy on λ_m is too small to observe in our experiment. The value of ν was taken to be 0.2, a typical value in solids, because ϵ does not depend sensitively on ν. With these approximations, the fit reproduced the experimental λ_m for both the SiO_2 and Al_2O_3 data and yielded $\gamma = 25 \pm 5$ mJ/m^2. Although γ between the M and I domains in VO_2 has not been measured previously, the value determined in our fit is comparable to structural domain wall energies in other oxide systems, such as ~35 mJ/m^2 for the 90° ferroelectric domain walls in $PbTiO_3$.[36]

It is important to emphasize one critical difference between the present nanobeam study and previous thin-film studies: the periodic domain pattern in VO_2 nanobeams is caused by a simple adhesive, nonepitaxial interaction between the nanobeam and the substrate. The exact nature of the nanobeam−substrate interface is not important, as long as the adhesion is sufficiently strong to prevent sliding from the substrate. This observation is in clear contrast to previous single-crystal and thin-film cases where, in the absence of epitaxial lattice control, disordered domain structures were observed.[3,4,10−13,37] The uniqueness of the present VO_2 nanobeam system originates from its geometry and single-crystallinity: the growth direction and high aspect ratio of the nanobeams ensures the uniaxial strain along the tetragonal *c* direction. Moreover, nanobeams do not support multiple domain structure along the width and height directions and thus behave as a one-dimensional system for M/I domain organization.

The present study demonstrates that a simple adhesive interaction between the nanobeam and the substrate changes the relative thermodynamic stability of M and I phases in VO_2 nanobeams and causes the spontaneous formation of periodic, alternating M−I domain patterns. It also shows that the spatial periodicity of these domains can be modified by changing the thickness of the nanobeam and the elasticity of the substrate. Most importantly, this study suggests that control over the morphology and growth direction of a single-crystalline nanostructure may provide a new strategy for strain engineering without the need for epitaxial growth from the substrate.

Acknowledgment. We thank M. Deshmukh, P. Pant, and Prof. Z. Suo for scientific discussions. This work is supported by NSF, Samsung Electronics, and the Packard Foundation.

Supporting Information Available: Experimental details for the synthesis and characterization techniques. Figures S1 and S2 show additional optical and KPM data. Figure S3 shows a plot of the lattice constant of VO_2 as a function of temperature. This material is available free of charge via the Internet at http://pubs.acs.org.

References

(1) Choi, K. J.; Biegalski, M.; Li, Y. L.; Sharan, A.; Schubert, J.; Uecker, R.; Reiche, P.; Chen, Y. B.; Pan, X. Q.; Gopalan, V.; Chen, L. Q.; Schlom, D. G.; Eom, C. B. *Science* **2004**, *306*, 1005−1009.
(2) Kwak, B. S.; Erbil, A.; Wilkens, B. J.; Budai, J. D.; Chisholm, M. F.; Boatner, L. A. *Phys. Rev. Lett.* **1992**, *68*, 3733−3736.

(3) Faeth, M.; Freisem, S.; Menovsky, A. A.; Tomioka, Y.; Aarts, J.; Mydosh, J. A. *Science* **1999**, *285*, 1540−1542.
(4) Mathur, N.; Littlewood, P. *Phys. Today* **2003**, *56*, 25−30.
(5) Ahn, K. H.; Lookman, T.; Bishop, A. R. *Nature* **2004**, *428*, 401−404.
(6) Locquet, J. P.; Perret, J.; Fompeyrine, J.; Maechler, E.; Seo, J. W.; van Tendeloo, G. *Nature* **1998**, *394*, 453−456.
(7) Speck, J. S.; Pompe, W. *J. Appl. Phys.* **1994**, *76*, 466−476.
(8) Streiffer, S. K.; Parker, C. B.; Romanov, A. E.; Lefevre, M. J.; Zhao, L.; Speck, J. S.; Pompe, W.; Foster, C. M.; Bai, G. R. *J. Appl. Phys.* **1998**, *83*, 2742−2753.
(9) Roytburd, A. L. *J. Appl. Phys.* **1998**, *83*, 239−245.
(10) Fisher, B. *J. Phys. C: Solid State Phys.* **1975**, *8*, 2072.
(11) Fisher, B. *J. Phys. C: Solid State Phys.* **1976**, *9*, 1201−1209.
(12) Valiev, K. A.; Mokerov, V. G.; Saraikin, V. V.; Petrova, A. G. *Sov. Phys. Solid State* **1977**, *19*, 1487−1491.
(13) Emelyanov, V. I.; Semenov, A. L. *Sov. Phys. Solid State* **1990**, *32*, 1790−1792.
(14) Dho, J.; Kim, Y. N.; Hwang, Y. S.; Kim, J. C.; Hur, N. H. *Appl. Phys. Lett.* **2003**, *82*, 1434−1436.
(15) Mott, N. F. *Metal−Insulator Transitions*, 1st ed.; Taylor & Francis: New York, 1974.
(16) Eyert, V. *Ann. Phys. (Berlin, Ger.)* **2002**, *11*, 650−702.
(17) Biermann, S.; Poteryaev, A.; Lichtenstein, A. I.; Georges, A. *Phys. Rev. Lett.* **2005**, *94*, 026404.
(18) Chudnovskiy, F.; Luryi, S.; Spivak, B. In *Future Trends in Microelectronics: The Nano Millenium*; Luryi, S., Xu, J. M., Zaslavsky, A., Eds.; Wiley-Interscience: Hoboken, NJ, 2002, p 148−155.
(19) Kim, H. T.; Chae, B. G.; Youn, D. H.; Maeng, S. L.; Kim, G.; Kang, K. Y.; Lim, Y. S. *New J. Phys.* **2004**, *6*, 51−59.
(20) Rakotoniaina, J. C.; Mokranitamellin, R.; Gavarri, J. R.; Vacquier, G.; Casalot, A.; Calvarin, G. *J. Solid State Chem.* **1993**, *103*, 81−94.
(21) Greenberg, C. B. *Thin Solid Films* **1994**, *251*, 81−83.
(22) Pouget, J. P.; Launois, H.; D'Haenens, J. P.; Merenda, P.; Rice, T. M. *Phys. Rev. Lett.* **1975**, *35*, 873−875.
(23) Lopez, R.; Feldman, L. C.; Haglund, R. F. *Phys. Rev. Lett.* **2004**, *93*, 177403.
(24) Wu, Y.; Xiang, J.; Yang, C.; Lu, W.; Lieber, C. M. *Nature* **2004**, *430*, 61−65.
(25) Guiton, B. S.; Gu, Q.; Prieto, A. L.; Gudiksen, M. S.; Park, H. *J. Am. Chem. Soc.* **2005**, *127*, 498−499.
(26) Kim, G. T.; Gu, G.; Waizmann, U.; Roth, S. *Appl. Phys. Lett.* **2002**, *80*, 1815−1817.
(27) Muraoka, Y.; Ueda, Y.; Hiroi, Z. *J. Phys. Chem. Solids* **2002**, *63*, 965−967.
(28) Bowman, R. M.; Gregg, J. M. *J. Mater. Sci.: Mater. Electron.* **1998**, *9*, 187−191.
(29) Nonnenmacher, M.; O'Boyle, M. P.; Wickramasinghe, H. K. *Appl. Phys. Lett.* **1991**, *58*, 2921−2923.
(30) Bonnell, D. A. *Scanning Probe Microscopy and Spectroscopy*, 2nd ed; Wiley-VCH: New York, 2000.
(31) Ono, S.; Takahashi, T. *Jpn. J. Appl. Phys.* **2004**, *43*, 4639−4642.
(32) Lopez, R.; Boatner, L. A.; Haynes, T. E.; Haglund, R. F.; Feldman, L. C. *Appl. Phys. Lett.* **2001**, *79*, 3161−3163.
(33) Kaganer, V. M.; Jenichen, B.; Schippan, F.; Braun, W.; Daweritz, L.; Ploog, K. H. *Phys. Rev. Lett.* **2000**, *85*, 341−344.
(34) Tsai, K. Y.; Chin, T. S.; Shieh, H. P. D. *Jpn. J. Appl. Phys., Part 1* **2004**, *43*, 6268−6273.
(35) Anderson, J. M.; Czigany, Z.; Jin, P.; Helmersson, U. *J. Vac. Sci. Technol., A* **2004**, *22*, 117−121.
(36) Meyer, B.; Vanderbilt, D. *Phys. Rev. B.* **2002**, *65*, 104111.
(37) Soh, Y. A.; Aeppli, G.; Kim, C. Y.; Mathur, N. D.; Blamire, M. G. *J. Appl. Phys.* **2003**, *93*, 8322−8324.

NL061831R